

Neural Ordinary Differential Equations

Ricky T. Q. Chen*, Yulia Rubanova*, Jesse Bettencourt*, David Duvenaud

University of Toronto, Vector Institute

Toronto, Canada

{rtqichen, rubanova, jessebett, duvenaud}@cs.toronto.edu

Abstract

We introduce a new family of deep neural network models. Instead of specifying a discrete sequence of hidden layers, we parameterize the derivative of the hidden state using a neural network. The output of the network is computed using a black-box differential equation solver. These continuous-depth models have constant memory cost, adapt their evaluation strategy to each input, and can explicitly trade numerical precision for speed. We demonstrate these properties in continuous-depth residual networks and continuous-time latent variable models. We also construct continuous normalizing flows, a generative model that can train by maximum likelihood, without partitioning or ordering the data dimensions. For training, we show how to scalably backpropagate through any ODE solver, without access to its internal operations. This allows end-to-end training of ODEs within larger models.

1 Introduction

Models such as residual networks, recurrent neural network decoders, and normalizing flows build complicated transformations by composing a sequence of transformations to a hidden state:

$$\mathbf{h}_{t+1} = \mathbf{h}_t + f(\mathbf{h}_t, \theta_t) \quad (1)$$

where $t \in \{0 \dots T\}$ and $\mathbf{h}_t \in \mathbb{R}^D$. These iterative updates can be seen as an Euler discretization of a continuous transformation (Lu et al., 2017; Haber and Ruthotto, 2017; Ruthotto and Haber, 2018).

What happens as we add more layers and take smaller steps? In the limit, we parameterize the continuous dynamics of hidden units using an ordinary differential equation (ODE) specified by a neural network:

$$\frac{d\mathbf{h}(t)}{dt} = f(\mathbf{h}(t), t, \theta) \quad (2)$$

Starting from the input layer $\mathbf{h}(0)$, we can define the output layer $\mathbf{h}(T)$ to be the solution to this ODE initial value problem at some time T . This value can be computed by a black-box differential equation solver, which evaluates the hidden unit dynamics f wherever necessary to determine the solution with the desired accuracy. Figure 1 contrasts these two approaches.

Defining and evaluating models using ODE solvers has several benefits:

Memory efficiency In Section 2, we show how to compute gradients of a scalar-valued loss with respect to all inputs of any ODE solver, *without backpropagating through the operations of the solver*. Not storing any intermediate quantities of the forward pass allows us to train our models with nearly constant memory cost as a function of depth, a major bottleneck of training deep models.

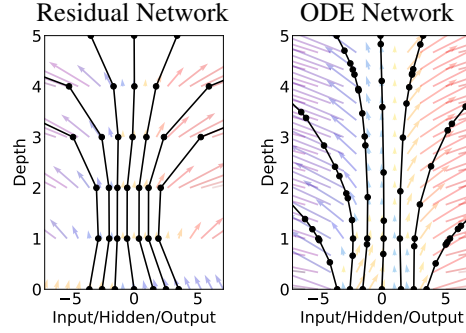


Figure 1: *Left:* A Residual network defines a discrete sequence of finite transformations. *Right:* A ODE network defines a vector field, which continuously transforms the state. *Both:* Circles represent evaluation locations.

Adaptive computation Euler’s method is perhaps the simplest method for solving ODEs. There have since been more than 120 years of development of efficient and accurate ODE solvers (Runge, 1895; Kutta, 1901; Hairer et al., 1987). Modern ODE solvers provide guarantees about the growth of approximation error, monitor the level of error, and adapt their evaluation strategy on the fly to achieve the requested level of accuracy. This allows the cost of evaluating a model to scale with problem complexity. After training, accuracy can be reduced for real-time or low-power applications.

Parameter efficiency When the hidden unit dynamics are parameterized as a continuous function of time, the parameters of nearby “layers” are automatically tied together. In Section 3, we show that this reduces the number of parameters required on a supervised learning task.

Scalable and invertible normalizing flows An unexpected side-benefit of continuous transformations is that the change of variables formula becomes easier to compute. In Section 4, we derive this result and use it to construct a new class of invertible density models that avoids the single-unit bottleneck of normalizing flows, and can be trained directly by maximum likelihood.

Continuous time-series models Unlike recurrent neural networks, which require discretizing observation and emission intervals, continuously-defined dynamics can naturally incorporate data which arrives at arbitrary times. In Section 5, we construct and demonstrate such a model.

2 Reverse-mode automatic differentiation of ODE solutions

The main technical difficulty in training continuous-depth networks is performing reverse-mode differentiation (also known as backpropagation) through the ODE solver. Differentiating through the operations of the forward pass is straightforward, but incurs a high memory cost and introduces additional numerical error.

We treat the ODE solver as a black box, and compute gradients using the *adjoint method* (Pontryagin et al., 1962). We present a modern proof of this method in Appendix B. This approach computes gradients by solving a second, augmented ODE backwards in time, and is applicable to all ODE solvers. This approach scales linearly with problem size, has low memory cost, and explicitly controls numerical error.

Consider optimizing a scalar-valued loss function $L()$, whose input is the result of an ODE solver:

$$L(\mathbf{z}(t_1)) = L \left(\int_{t_0}^{t_1} f(\mathbf{z}(t), t, \theta) dt \right) = L(\text{ODESolve}(\mathbf{z}(t_0), f, t_0, t_1, \theta)) \quad (3)$$

To optimize L , we require gradients with respect to its parameters: $\mathbf{z}(t_0)$, t_0 , t_1 , and θ . The first step is to determine how the gradient of the loss depends on the hidden state $\mathbf{z}(t)$ at each instant. This quantity is called the *adjoint* $a(t) = -\partial L / \partial \mathbf{z}(t)$. Its dynamics are given by another ODE, which can be thought of as the instantaneous analog of the chain rule:

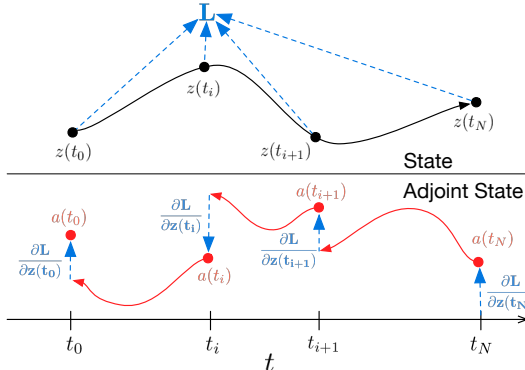


Figure 2: Reverse-mode differentiation through an ODE solver requires solving an augmented system backwards in time. This adjoint state is updated by the gradient at each observation.

$$\frac{da(t)}{dt} = -a(t)^\top \frac{\partial f(\mathbf{z}(t), t, \theta)}{\partial \mathbf{z}} \quad (4)$$

We can compute $\partial L / \partial \mathbf{z}(t_0)$ by another call to an ODE solver. This solver must run backwards, starting from the “initial value” of $\partial L / \partial \mathbf{z}(t_1)$. One complication is that solving this ODE requires the knowing value of $\mathbf{z}(t)$ along its entire trajectory. However, we can simply recompute $\mathbf{z}(t)$ backwards in time together with the adjoint, starting from its final value $\mathbf{z}(t_1)$.

Computing the gradients with respect to the parameters θ requires evaluating a third integral, which depends on both $\mathbf{z}(t)$ and $a(t)$:

$$\frac{dL}{d\theta} = \int_{t_1}^{t_0} a(t)^\top \frac{\partial f(\mathbf{z}(t), t, \theta)}{\partial \theta} dt \quad (5)$$

All three of these integrals can be computed in a single call to an ODE solver, which concatenates the original state, the adjoint, and the other partial derivatives into a single vector. Algorithm 1 shows how to construct the necessary dynamics, and call an ODE solver to compute all gradients at once.

Algorithm 1 Reverse-mode derivative of an ODE initial value problem

Input: dynamics parameters θ , start time t_0 , stop time t_1 , final state $\mathbf{z}(t_1)$, loss gradient $\partial L / \partial \mathbf{z}(t_1)$

$$\frac{\partial L}{\partial t_1} = \frac{\partial L}{\partial \mathbf{z}(t_1)}^\top f(\mathbf{z}(t_1), t_1, \theta) \quad \triangleright \text{Compute gradient w.r.t. } t_1$$

$$s_0 = [\mathbf{z}(t_1), \frac{\partial L}{\partial \mathbf{z}(t_1)}, \mathbf{0}, -\frac{\partial L}{\partial t_1}] \quad \triangleright \text{Define initial augmented state}$$

def `aug_dynamics`($[\mathbf{z}(t), \mathbf{a}(t), -, -], t, \theta$): \triangleright Define dynamics on augmented state

return $[f(\mathbf{z}(t), t, \theta), -\mathbf{a}(t)^\top \frac{\partial f}{\partial \mathbf{z}}, -\mathbf{a}(t)^\top \frac{\partial f}{\partial \theta}, -\mathbf{a}(t)^\top \frac{\partial f}{\partial t}] \quad \triangleright$ Concatenate time-derivatives

$$[\mathbf{z}(t_0), \frac{\partial L}{\partial \mathbf{z}(t_0)}, \frac{\partial L}{\partial \theta}, \frac{\partial L}{\partial t_0}] = \text{ODESolve}(s_0, \text{aug_dynamics}, t_1, t_0, \theta) \quad \triangleright \text{Solve reverse-time ODE}$$

return $\frac{\partial L}{\partial \mathbf{z}(t_0)}, \frac{\partial L}{\partial \theta}, \frac{\partial L}{\partial t_0}, \frac{\partial L}{\partial t_1} \quad \triangleright \text{Return all gradients}$

Most ODE solvers have the option to output the state $\mathbf{z}(t)$ at multiple times. When the loss depends on these intermediate states, the reverse-mode derivative must be broken into a sequence of separate solves, one between each consecutive pair of outputs (Figure 2). At each observation, the adjoint must be adjusted by the corresponding direct gradient $\partial L / \partial \mathbf{z}(t_i)$.

The results above extend those of Stapor et al. (2018, section 2.4.2). Detailed derivations are provided in Appendix B. Appendix C provides Python code which computes all derivatives for `scipy.integrate.odeint` by extending the `autograd` automatic differentiation package. This code also supports all higher-order derivatives.

3 Replacing residual networks with ODEs for supervised learning

In this section, we experimentally investigate the training of neural ODEs for supervised learning.

Software To solve ODE initial value problems numerically, we use the implicit Adams method implemented in LSODE and VODE and interfaced through the `scipy.integrate` package. Being an implicit method, it has better guarantees than explicit methods such as Runge-Kutta but requires solving a nonlinear optimization problem at every step. This setup makes direct backpropagation through the integrator difficult. We implement the adjoint sensitivity method in Python’s `autograd` framework (Maclaurin et al., 2015). For the experiments in this section, we evaluated the hidden state dynamics and their derivatives on the GPU using Tensorflow, which were then called from the Fortran ODE solvers, which were called from Python `autograd` code.

Model Architectures We experiment with a small residual network which downsamples the input twice then applies 6 residual blocks, which are replaced by an `ODESolve` module in the ODE-Net variant. We also test a network which directly backpropagates through a Runge-Kutta integrator, referred to as RK-Net.

Table 1 shows test error, number of parameters, and memory cost. L denotes the number of layers in the ResNet, and \tilde{L} is the number of function evaluations that the ODE solver requests in a single forward pass, which can be interpreted as an implicit number of layers.

We find that ODE-Nets and RK-Nets can achieve around the same performance as the ResNet, while using fewer parameters. For reference, a neural net with a single hidden layer of 300 units has around the same number of parameters as the ODE-Net and RK-Net architecture that we tested.

Table 1: Performance on MNIST. [†]From LeCun et al. (1998).

	Test Error	# Params	Memory	Time
1-Layer MLP [†]	1.60%	0.24 M	-	-
ResNet	0.41%	0.60 M	$\mathcal{O}(L)$	$\mathcal{O}(L)$
RK-Net	0.47%	0.22 M	$\mathcal{O}(\tilde{L})$	$\mathcal{O}(\tilde{L})$
ODE-Net	0.42%	0.22 M	$\mathcal{O}(1)$	$\mathcal{O}(\tilde{L})$

Error Control in ODE-Nets ODE solvers can approximately ensure that the output is within a given tolerance of the true solution. Changing this tolerance changes the behavior of the network.

We first verify that error can indeed be controlled in Figure 3a. The time spent by the forward call is proportional to the number of function evaluations (Figure 3b), so tuning the tolerance gives us a trade-off between accuracy and computational cost. One could train with high accuracy, but switch to a lower accuracy at test time.

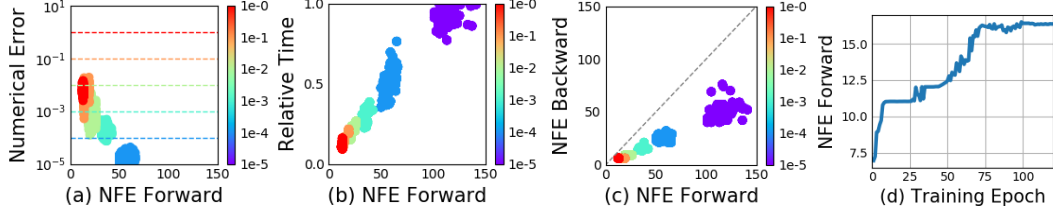


Figure 3: Statistics of a trained ODE-Net. (NFE = number of function evaluations.)

Figure 3c) shows a surprising result: the number of evaluations in the backward pass is roughly half of the forward pass. This suggests that the adjoint sensitivity method is not only more memory efficient, but also more computationally efficient than directly backpropagating through the integrator, because the latter approach will need to backprop through each function evaluation in the forward pass.

Network Depth It’s not clear how to define the ‘depth’ of an ODE solution. A related quantity is the number of evaluations of the hidden state dynamics required, a detail delegated to the ODE solver and dependent on the initial state or input. Figure 3d shows that he number of function evaluations increases throughout training, presumably adapting to increasing complexity of the model.

4 Continuous Normalizing Flows

The discretized equation (1) also appears in normalizing flows (Rezende and Mohamed, 2015) and the NICE framework (Dinh et al., 2014). These methods use the change of variables theorem to compute exact changes in probability if samples are transformed through a bijective function f :

$$\mathbf{z}_1 = f(\mathbf{z}_0) \implies \log p(\mathbf{z}_1) = \log p(\mathbf{z}_0) - \log \left| \det \frac{\partial f}{\partial \mathbf{z}_0} \right| \quad (6)$$

An example is the planar normalizing flow (Rezende and Mohamed, 2015):

$$\mathbf{z}(t+1) = \mathbf{z}(t) + uh(w^\top \mathbf{z}(t) + b), \quad \log p(\mathbf{z}(t+1)) = \log p(\mathbf{z}(t)) - \log \left| 1 + u^\top \frac{\partial h}{\partial \mathbf{z}} \right| \quad (7)$$

Generally, the main bottleneck to using the change of variables formula is computing of the determinant of the Jacobian $\partial f / \partial \mathbf{z}$, which has a cubic cost in either the dimension of \mathbf{z} , or the number of hidden units. Recent work explores the tradeoff between the expressiveness of normalizing flow layers and computational cost (Kingma et al., 2016; Tomczak and Welling, 2016; Berg et al., 2018).

Surprisingly, moving from a discrete set of layers to a continuous transformation simplifies the computation of the change in normalizing constant:

Theorem 1 (Instantaneous Change of Variables). *Let $\mathbf{z}(t)$ be a finite continuous random variable with probability $p(\mathbf{z}(t))$ dependent on time. Let $\frac{d\mathbf{z}}{dt} = f(\mathbf{z}(t), t)$ be a differential equation describing a continuous-in-time transformation of $\mathbf{z}(t)$. Assuming that f is uniformly Lipschitz continuous in \mathbf{z} and continuous in t , then the change in log probability also follows a differential equation,*

$$\frac{\partial \log p(\mathbf{z}(t))}{\partial t} = -\text{tr} \left(\frac{df}{d\mathbf{z}(t)} \right) \quad (8)$$

Proof in Appendix A. Instead of the log determinant in (6), we now only require a trace operation. Also unlike standard finite flows, the differential equation f does not need to be bijective, since if uniqueness is satisfied, then the entire transformation is automatically bijective.

As an example application of the instantaneous change of variables, we can examine the continuous analog of the planar flow, and its change in normalization constant:

$$\frac{d\mathbf{z}(t)}{dt} = uh(w^\top \mathbf{z}(t) + b), \quad \frac{\partial \log p(\mathbf{z}(t))}{\partial t} = -u^\top \frac{\partial h}{\partial \mathbf{z}(t)} \quad (9)$$

Given an initial distribution $p(\mathbf{z}(0))$, we can sample from $p(\mathbf{z}(t))$ and evaluate its density by solving this combined ODE.

Using multiple hidden units with linear cost While \det is not a linear function, the trace function is, which implies $\text{tr}(\sum_n J_n) = \sum_n \text{tr}(J_n)$. Thus if our dynamics is given by a sum of functions then the differential equation for the log density is also a sum:

$$\frac{d\mathbf{z}(t)}{dt} = \sum_{n=1}^M f_n(\mathbf{z}(t)), \quad \frac{d \log p(\mathbf{z}(t))}{dt} = \sum_{n=1}^M \text{tr}\left(\frac{\partial f_n}{\partial \mathbf{z}}\right) \quad (10)$$

This means we can cheaply evaluate flow models having many hidden units, with a cost only linear in the number of hidden units M . Evaluating such ‘wide’ flow layers using standard normalizing flows costs $\mathcal{O}(M^3)$, meaning that standard NF architectures use many layers of only a single hidden unit.

Time-dependent dynamics We can specify the parameters of a flow as a function of t , making the differential equation $f(\mathbf{z}(t), t)$ change with t . This is parameterization is a kind of hypernetwork (Ha et al., 2016). We also introduce a gating mechanism for each hidden unit, $\frac{d\mathbf{z}}{dt} = \sum_n \sigma_n(t) f_n(\mathbf{z})$ where $\sigma_n(t) \in (0, 1)$ is a neural network that learns when the dynamic $f_n(\mathbf{z})$ should be applied. We call these models continuous normalizing flows (CNF).

4.1 Experiments with Continuous Normalizing Flows

We first compare continuous and discrete planar flows at learning to sample from a known distribution. We show that a planar CNF with M hidden units can be at least as expressive as a planar NF with $K = M$ layers, and sometimes much more expressive.

Density matching We configure the CNF as described above, and train for 10,000 iterations using Adam (Kingma and Ba, 2014). In contrast, the NF is trained for 500,000 iterations using RMSprop (Hinton et al., 2012), as suggested by Rezende and Mohamed (2015). For this task, we minimize $\text{KL}(q(\mathbf{x}) \| p(\mathbf{x}))$ as the loss function where q is the flow model and the target density $p(\cdot)$ can be evaluated. Figure 4 shows that CNF generally achieves lower loss.

Maximum Likelihood Training A useful property of continuous-time normalizing flows is that we can compute the reverse transformation for about the same cost as the forward pass, which cannot be said for normalizing flows. This lets us train the flow on a density estimation task by performing

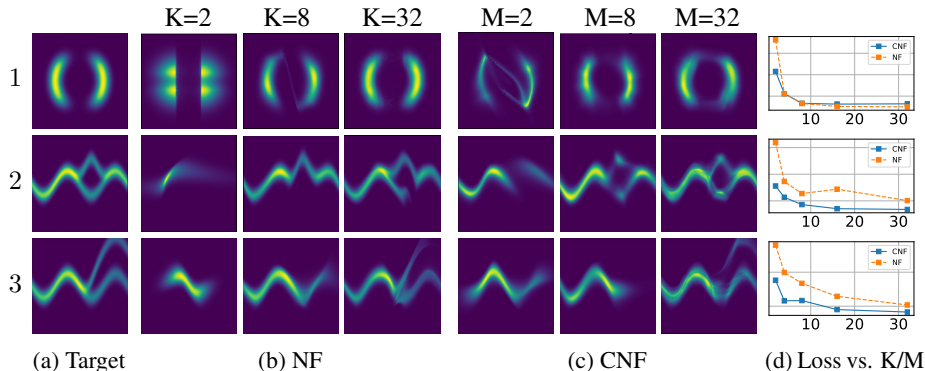


Figure 4: Comparison of normalizing flows versus continuous normalizing flows. The model capacity of normalizing flows is determined by their depth (K), while continuous normalizing flows can also increase capacity by increasing width (M), making them easier to train.

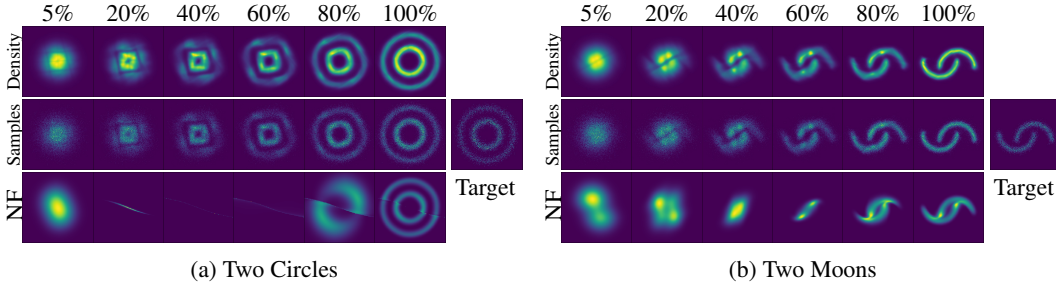


Figure 5: **Visualizing the transformation from noise to data.** Continuous-time normalizing flows are reversible, so we can train on a density estimation task and still be able to sample from the learned density efficiently.

maximum likelihood estimation, which maximizes $\mathbb{E}_{p(\mathbf{x})}[\log q(\mathbf{x})]$ where $q(\cdot)$ is computed using the appropriate change of variables theorem, then afterwards reverse the CNF to generate random samples from $q(\mathbf{x})$.

For this task, we use 64 hidden units for CNF, and 64 stacked one-hidden-unit layers for NF. Figure 5 shows the learned dynamics. Instead of showing the initial Gaussian distribution, we display the transformed distribution after a small amount of time which shows the locations of the initial planar flows. Interestingly, to fit the Two Circles distribution, the CNF rotates the planar flows so that the particles can be evenly spread into circles. While the CNF transformations are smooth and interpretable, we find that NF transformations are very unintuitive and this model has difficulty fitting the two moons dataset in Figure 5b.

5 A generative latent function time-series model

Applying neural networks to irregularly-sampled data such as medical records, network traffic, or neural spiking data is difficult. Typically, observations are put into bins of fixed duration, and the latent dynamics are discretized in the same way. This leads to difficulties with missing data and ill-defined latent variables. Missing data can be addressed using generative time-series models (Álvarez and Lawrence, 2011; Futoma et al., 2017; Mei and Eisner, 2017; Soleimani et al., 2017a) or data imputation (Che et al., 2018). Another approach concatenates time-stamp information to the input of an RNN (Choi et al., 2016; Lipton et al., 2016; Du et al., 2016; Li, 2017).

We present a continuous-time, generative approach to modeling time series. Our model represents each time series by a latent trajectory. Each trajectory is determined from a local initial state, \mathbf{z}_{t_0} , and a global set of latent dynamics shared across all time series. Given observation times t_0, t_1, \dots, t_N and an initial state \mathbf{z}_{t_0} , an ODE solver produces $\mathbf{z}_{t_1}, \dots, \mathbf{z}_{t_N}$, which describe the latent state at each observation. We define this generative model formally through a sampling procedure:

$$\mathbf{z}_{t_0} \sim p(\mathbf{z}_{t_0}) \quad (11)$$

$$\mathbf{z}_{t_1}, \mathbf{z}_{t_2}, \dots, \mathbf{z}_{t_N} = \text{ODESolve}(\mathbf{z}_{t_0}, f, \theta_f, t_0, \dots, t_N) \quad (12)$$

$$\text{each } \mathbf{x}_{t_i} \sim p(\mathbf{x}|\mathbf{z}_{t_i}, \theta_x) \quad (13)$$

Function f is a time-invariant function that takes the value \mathbf{z} at the current time step and outputs the gradient: $\partial \mathbf{z}(t)/\partial t = f(\mathbf{z}(t), \theta_f)$. We parametrize this function using a neural net. Because f is time-invariant, given any latent state $\mathbf{z}(t)$, the entire latent trajectory is uniquely defined. Extrapolating this latent trajectory lets us make predictions arbitrarily far forwards or backwards in time.

Training and Prediction We can train this latent-variable model as a variational autoencoder (Kingma and Welling, 2014; Rezende et al., 2014), with sequence-valued observations. Our recognition net is an RNN, which consumes the data sequentially backwards in time, and outputs $q_\phi(\mathbf{z}_0|\mathbf{x}_1, \mathbf{x}_2, \dots, \mathbf{x}_N)$. A detailed algorithm can be found in Appendix D. Using ODEs as a

Animated Figures 4 and 5 available at: <http://www.cs.toronto.edu/~jessebett/nodes/>

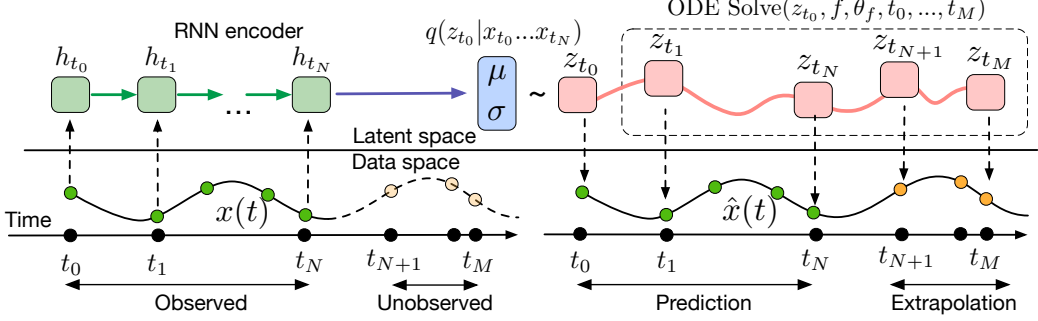


Figure 6: Computation graph of the latent ODE model.

generative model allows us to make predictions for arbitrary time points $t_1 \dots t_M$ on a continuous timeline.

Poisson Process likelihoods The fact that an observation occurred often tells us something about the latent state. For example, a patient may be more likely to take a medical test if they are sick. The rate of events can be parameterized by a function of the latent state: $p(\text{event at time } t | \mathbf{z}(t)) = \lambda(\mathbf{z}(t))$. Given this rate function, the likelihood of a set of independent observation times in the interval $[t_{\text{start}}, t_{\text{end}}]$ is given by an inhomogeneous Poisson process (Palm, 1943):

$$\log p(t_1 \dots t_N | t_{\text{start}}, t_{\text{end}}) = \sum_{i=1}^N \log \lambda(\mathbf{z}(t_i)) - \int_{t_{\text{start}}}^{t_{\text{end}}} \lambda(\mathbf{z}(t)) dt$$

We can parameterize $\lambda(\cdot)$ using another neural network. Conveniently, we can evaluate both the latent trajectory and the Poisson process likelihood together in a single call to an ODE solver. Figure 7 shows the event rate learned by such a model on a toy dataset.

A Poisson process likelihood on observations can be combined with an event rate can easily be combined with a data likelihood to give a joint distribution over observations and their times.

5.1 Time-series Latent ODE Experiments

We investigate the ability of the latent ODE model to fit and extrapolate time series. The recognition network is an RNN with 25 hidden units. We use a 4-dimensional latent space. We parameterize the dynamics function f with a one-hidden-layer network with 20 hidden units. The decoder computing $p(\mathbf{x}_{t_i} | \mathbf{z}_{t_i})$ is another neural network with one hidden layer with 20 hidden units. Our baseline was a recurrent neural net with 25 hidden units trained to minimize negative Gaussian log-likelihood. We trained a second version of this RNN whose inputs were concatenated with the time difference to the next observation to aid RNN with irregular observations.

Bi-directional spiral dataset We generated a dataset of 1000 2-dimensional spirals, each starting at a different point, sampled at 100 equally-spaced timesteps. The dataset contains two types of spirals: half are clockwise while the other half counter-clockwise. To make the task more realistic, we add gaussian noise to the observations.

Time series with irregular time points To generate irregular timestamps, we randomly sample points from each trajectory without replacement ($n = \{30, 50, 100\}$). We report predictive root-mean-squared error (RMSE) on 100 time points extending beyond those that were used for training. Table 2 shows that the latent ODE has substantially lower predictive RMSE.

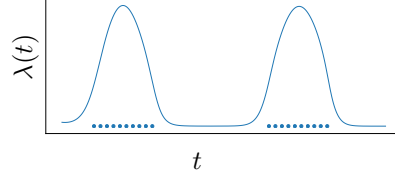


Figure 7: Fitting a latent ODE dynamics model with a Poisson process likelihood. Dots show event times. The line is the learned intensity $\lambda(t)$ of the Poisson process.

Table 2: Predictive RMSE on test set

# Observations	30/100	50/100	100/100
RNN	0.3937	0.3202	0.1813
Latent ODE	0.1642	0.1502	0.1346



Figure 9: Data-space trajectories decoded from varying one dimension of \mathbf{z}_{t_0} . Color indicates progression through time, starting at purple and ending at red. Note that the trajectories on the left are counter-clockwise, while the trajectories on the right are clockwise.

Figure 8 shows examples of spiral reconstructions with 30 sub-sampled points. Reconstructions from the latent ODE were obtained by sampling from the posterior over latent trajectories and decoding it to data-space. Examples with varying number of time points are shown in Appendix E. We observed that reconstructions and extrapolations are consistent with the ground truth regardless of number of observed points and despite the noise.

Latent space interpolation Figure 8c shows latent trajectories projected onto the first two dimensions of the latent space. The trajectories form two separate clusters of trajectories, one decoding to clockwise spirals, the other to counter-clockwise. Figure 9 shows that the latent trajectories change smoothly as a function of the initial point $\mathbf{z}(t_0)$, switching from a clockwise to a counter-clockwise spiral.

6 Scope and Limitations

Minibatching Second, the use of minibatches is less straightforward than for standard neural networks. One can still batch together evaluations through the ODE solver by concatenating the states of each batch element together, creating a combined ODE with dimension $D \times K$. In some cases, controlling error on all batch elements together might require evaluating the combined system K times more often than if each system was solved individually, leading to a more than $\mathcal{O}(K)$ cost to evaluate K batch elements. However, in practice the number of evaluations did not increase substantially when using minibatches.

Uniqueness When do continuous dynamics have a unique solution? Picard's existence theorem (Coddington and Levinson, 1955) states that the solution to an initial value problem exists and is unique if the differential equation is uniformly Lipschitz continuous in \mathbf{z} and continuous in t . This theorem holds for our model if the neural network has finite weights and uses Lipschitz nonlinearities, such as `tanh` or `relu`.

Reversibility Even if the forward trajectory is invertible in principle, in practice there will be three compounding sources of error in the gradient: 1) Numerical error introduced in the forward ODE solver; 2) Information lost due to multiple initial values mapping to the same final state; and 3) Numerical error introduced in the reverse ODE solver.

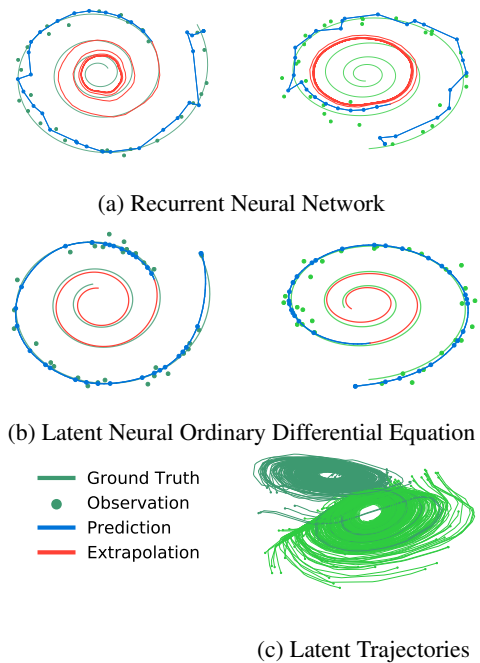


Figure 8: (a): Reconstruction and extrapolation of spirals with irregular time points by a recurrent neural network. (b): Reconstructions and extrapolations by a latent neural ODE. Blue curve shows model prediction. Red shows extrapolation. (c) A projection of inferred 4-dimensional latent ODE trajectories onto their first two dimensions. Color indicates the direction of the corresponding trajectory. The model has learned latent dynamics which distinguishes the two directions.

Error from 1 and 3 can be made as small as desired, at the cost of more computation. Error from 2 could be expected to be a problem if the system dynamics encoded optimization-like, convergent dynamics. Note that exactly convergent transformations are disallowed by Lipschitz dynamics. In our experiments we did not find this to be a practical problem, and we informally checked that reversing many layers of continuous normalizing flows recovered the initial Gaussian density.

If necessary, exact reversibility could be recovered by storing the initial state and solving the reverse pass as a boundary-value problem instead of as an initial-value problem. If truly convergent dynamics are required, replacing the ODE solver with a differentiable black-box optimizer, as in OptNet (Amos and Kolter, 2017), would be more appropriate.

7 Related Work

The interpretation of residual networks He et al. (2016) as approximate ODE solvers spurred research into exploiting reversibility and approximate computation in ResNets (Chang et al., 2017; Lu et al., 2017). We demonstrate these same properties in more generality by directly using an ODE solver.

Adaptive computation One can adapt computation time by training secondary neural networks to choose the number of evaluations of recurrent or residual networks (Graves, 2016; Jernite et al., 2016; Figurnov et al., 2017; Chang et al., 2018). However, this introduces overhead both at training and test time, and extra parameters that need to be fit. In contrast, ODE solvers offer well-studied, computationally cheap, and generalizable rules for adapting the amount of computation.

Reversibility Recent work developed reversible versions of residual networks (Gomez et al., 2017; Haber and Ruthotto, 2017; Chang et al., 2017), which gives the same memory savings as our approach. However, this method requires the use of restricted architectures which partition the hidden units. Our approach does not have these restrictions.

Learning differential equations Much recent work has proposed learning differential equations from data. One can train feed-forward or recurrent neural networks to approximate a differential equation (Raissi and Karniadakis, 2018; Raissi et al., 2018a; Long et al., 2017), with applications such as fluid simulation (Wiewel et al., 2018). There is also significant work on connecting Gaussian Processes (GPs) and ODE solvers (Schober et al., 2014). GPs have been adapted to fit differential equations (Raissi et al., 2018b) and can naturally model continuous-time effects and interventions (Soleimani et al., 2017b; Schulam and Saria, 2017). Ryder et al. (2018) use stochastic variational inference to recover the solution of a given stochastic differential equation.

Differentiating through ODE solvers The dolfin library (Farrell et al., 2013) implements adjoint computation for general ODE and PDE solutions, but only by backpropagating through the individual operations of the forward solver. The Stan library (Carpenter et al., 2015) implements gradient estimation through ODE solutions using forward sensitivity analysis. However, forward sensitivity analysis is quadratic-time in the number of variables, whereas the adjoint sensitivity analysis is linear (Carpenter et al., 2015; Zhang and Sandu, 2014). Melicher et al. (2017) used the adjoint method to train bespoke latent dynamic models.

In contrast, by providing a generic vector-Jacobian product, we allow an ODE solver to be trained end-to-end with any other differentiable model components. While use of vector-Jacobian products for solving the adjoint method has been explored in optimal control (Andersson, 2013), we explore a fully general integration of black-box ODE solvers into automatic differentiation (Baydin et al., 2018) and highlight its potential in deep learning and generative modeling.

8 Conclusion

We investigated the use of black-box ODE solvers as a model component, developing new models for time-series modeling, supervised learning, and density estimation. These models are evaluated adaptively, and allow explicit control of the tradeoff between computation speed and accuracy. Finally, we derived an instantaneous version of the change of variables formula, and developed continuous-time normalizing flows, which can scale to large layer sizes.

9 Acknowledgements

We thank Wenyi Wang and Geoff Roeder for help with proofs, and Daniel Duckworth, Ethan Fetaya, Hossein Soleimani, Eldad Haber, Ken Caluwaerts, and Daniel Flam-Shepherd for feedback on early drafts. We thank Chris Rackauckas, Dougal Maclaurin, and Matthew James Johnson for helpful discussions.

References

- Mauricio A Álvarez and Neil D Lawrence. Computationally efficient convolved multiple output Gaussian processes. *Journal of Machine Learning Research*, 12(May):1459–1500, 2011.
- Brandon Amos and J Zico Kolter. OptNet: Differentiable optimization as a layer in neural networks. In *International Conference on Machine Learning*, pages 136–145, 2017.
- Joel Andersson. *A general-purpose software framework for dynamic optimization*. PhD thesis, 2013.
- Atilim Gunes Baydin, Barak A Pearlmutter, Alexey Andreyevich Radul, and Jeffrey Mark Siskind. Automatic differentiation in machine learning: a survey. *Journal of machine learning research*, 18(153):1–153, 2018.
- Rianne van den Berg, Leonard Hasenclever, Jakub M Tomczak, and Max Welling. Sylvester normalizing flows for variational inference. *arXiv preprint arXiv:1803.05649*, 2018.
- Bob Carpenter, Matthew D Hoffman, Marcus Brubaker, Daniel Lee, Peter Li, and Michael Betancourt. The Stan math library: Reverse-mode automatic differentiation in c++. *arXiv preprint arXiv:1509.07164*, 2015.
- Bo Chang, Lili Meng, Eldad Haber, Lars Ruthotto, David Begert, and Elliot Holtham. Reversible architectures for arbitrarily deep residual neural networks. *arXiv preprint arXiv:1709.03698*, 2017.
- Bo Chang, Lili Meng, Eldad Haber, Frederick Tung, and David Begert. Multi-level residual networks from dynamical systems view. In *International Conference on Learning Representations*, 2018. URL <https://openreview.net/forum?id=SyJS-OgR->.
- Zhengping Che, Sanjay Purushotham, Kyunghyun Cho, David Sontag, and Yan Liu. Recurrent neural networks for multivariate time series with missing values. *Scientific Reports*, 8(1):6085, 2018. URL <https://doi.org/10.1038/s41598-018-24271-9>.
- Edward Choi, Mohammad Taha Bahadori, Andy Schuetz, Walter F. Stewart, and Jimeng Sun. Doctor AI: Predicting clinical events via recurrent neural networks. In *Proceedings of the 1st Machine Learning for Healthcare Conference*, volume 56 of *Proceedings of Machine Learning Research*, pages 301–318. PMLR, 18–19 Aug 2016. URL <http://proceedings.mlr.press/v56/Choi16.html>.
- Earl A Coddington and Norman Levinson. *Theory of ordinary differential equations*. Tata McGraw-Hill Education, 1955.
- Laurent Dinh, David Krueger, and Yoshua Bengio. NICE: Non-linear independent components estimation. *arXiv preprint arXiv:1410.8516*, 2014.
- Nan Du, Hanjun Dai, Rakshit Trivedi, Utkarsh Upadhyay, Manuel Gomez-Rodriguez, and Le Song. Recurrent marked temporal point processes: Embedding event history to vector. In *International Conference on Knowledge Discovery and Data Mining*, pages 1555–1564. ACM, 2016.
- Patrick Farrell, David Ham, Simon Funke, and Marie Rognes. Automated derivation of the adjoint of high-level transient finite element programs. *SIAM Journal on Scientific Computing*, 2013.
- Michael Figurnov, Maxwell D Collins, Yukun Zhu, Li Zhang, Jonathan Huang, Dmitry Vetrov, and Ruslan Salakhutdinov. Spatially adaptive computation time for residual networks. *arXiv preprint*, 2017.
- J. Futoma, S. Hariharan, and K. Heller. Learning to Detect Sepsis with a Multitask Gaussian Process RNN Classifier. *ArXiv e-prints*, 2017.

- Aidan N Gomez, Mengye Ren, Raquel Urtasun, and Roger B Grosse. The reversible residual network: Backpropagation without storing activations. In *Advances in Neural Information Processing Systems*, pages 2211–2221, 2017.
- Alex Graves. Adaptive computation time for recurrent neural networks. *arXiv preprint arXiv:1603.08983*, 2016.
- David Ha, Andrew Dai, and Quoc V Le. Hypernetworks. *arXiv preprint arXiv:1609.09106*, 2016.
- Eldad Haber and Lars Ruthotto. Stable architectures for deep neural networks. *Inverse Problems*, 34(1):014004, 2017.
- E. Hairer, S.P. Nørsett, and G. Wanner. *Solving Ordinary Differential Equations I – Nonstiff Problems*. Springer, 1987.
- Kaiming He, Xiangyu Zhang, Shaoqing Ren, and Jian Sun. Deep residual learning for image recognition. In *Proceedings of the IEEE conference on computer vision and pattern recognition*, pages 770–778, 2016.
- Geoffrey Hinton, Nitish Srivastava, and Kevin Swersky. Neural networks for machine learning lecture 6a overview of mini-batch gradient descent, 2012.
- Yacine Jernite, Edouard Grave, Armand Joulin, and Tomas Mikolov. Variable computation in recurrent neural networks. *arXiv preprint arXiv:1611.06188*, 2016.
- Diederik P Kingma and Jimmy Ba. Adam: A method for stochastic optimization. *arXiv preprint arXiv:1412.6980*, 2014.
- Diederik P. Kingma and Max Welling. Auto-encoding variational Bayes. *International Conference on Learning Representations*, 2014.
- Diederik P Kingma, Tim Salimans, Rafal Jozefowicz, Xi Chen, Ilya Sutskever, and Max Welling. Improved variational inference with inverse autoregressive flow. In *Advances in Neural Information Processing Systems*, pages 4743–4751, 2016.
- W. Kutta. Beitrag zur näherungsweisen Integration totaler Differentialgleichungen. *Zeitschrift für Mathematik und Physik*, 46:435–453, 1901.
- Yann LeCun, Léon Bottou, Yoshua Bengio, and Patrick Haffner. Gradient-based learning applied to document recognition. *Proceedings of the IEEE*, 86(11):2278–2324, 1998.
- Yang Li. Time-dependent representation for neural event sequence prediction. *arXiv preprint arXiv:1708.00065*, 2017.
- Zachary C Lipton, David Kale, and Randall Wetzel. Directly modeling missing data in sequences with RNNs: Improved classification of clinical time series. In *Proceedings of the 1st Machine Learning for Healthcare Conference*, volume 56 of *Proceedings of Machine Learning Research*, pages 253–270. PMLR, 18–19 Aug 2016. URL <http://proceedings.mlr.press/v56/Lipton16.html>.
- Z. Long, Y. Lu, X. Ma, and B. Dong. PDE-Net: Learning PDEs from Data. *ArXiv e-prints*, 2017.
- Yiping Lu, Aoxiao Zhong, Quanzheng Li, and Bin Dong. Beyond finite layer neural networks: Bridging deep architectures and numerical differential equations. *arXiv preprint arXiv:1710.10121*, 2017.
- Dougal Maclaurin, David Duvenaud, and Ryan P Adams. Autograd: Reverse-mode differentiation of native Python. In *ICML workshop on Automatic Machine Learning*, 2015.
- Hongyuan Mei and Jason M Eisner. The neural Hawkes process: A neurally self-modulating multivariate point process. In *Advances in Neural Information Processing Systems*, pages 6757–6767, 2017.
- Valdemar Melicher, Tom Haber, and Wim Vanroose. Fast derivatives of likelihood functionals for ODE based models using adjoint-state method. *Computational Statistics*, 32(4):1621–1643, 2017.

- Conny Palm. Intensitätsschwankungen im fernsprechverkehr. *Ericsson Technics*, 1943.
- Lev Semenovich Pontryagin, EF Mishchenko, VG Boltyanskii, and RV Gamkrelidze. The mathematical theory of optimal processes. 1962.
- M. Raissi and G. E. Karniadakis. Hidden physics models: Machine learning of nonlinear partial differential equations. *Journal of Computational Physics*, pages 125–141, 2018.
- Maziar Raissi, Paris Perdikaris, and George Em Karniadakis. Multistep neural networks for data-driven discovery of nonlinear dynamical systems. *arXiv preprint arXiv:1801.01236*, 2018a.
- Maziar Raissi, Paris Perdikaris, and George Em Karniadakis. Numerical Gaussian processes for time-dependent and nonlinear partial differential equations. *SIAM Journal on Scientific Computing*, 40(1):A172–A198, 2018b.
- Danilo J Rezende, Shakir Mohamed, and Daan Wierstra. Stochastic backpropagation and approximate inference in deep generative models. In *Proceedings of the 31st International Conference on Machine Learning*, pages 1278–1286, 2014.
- Danilo Jimenez Rezende and Shakir Mohamed. Variational inference with normalizing flows. *arXiv preprint arXiv:1505.05770*, 2015.
- C. Runge. Über die numerische Auflösung von Differentialgleichungen. *Mathematische Annalen*, 46: 167–178, 1895.
- Lars Ruthotto and Eldad Haber. Deep neural networks motivated by partial differential equations. *arXiv preprint arXiv:1804.04272*, 2018.
- T. Ryder, A. Golightly, A. S. McGough, and D. Prangle. Black-box Variational Inference for Stochastic Differential Equations. *ArXiv e-prints*, 2018.
- Michael Schober, David Duvenaud, and Philipp Hennig. Probabilistic ODE solvers with Runge-Kutta means. In *Advances in Neural Information Processing Systems* 25, 2014.
- Peter Schulam and Suchi Saria. What-if reasoning with counterfactual Gaussian processes. *arXiv preprint arXiv:1703.10651*, 2017.
- Hossein Soleimani, James Hensman, and Suchi Saria. Scalable joint models for reliable uncertainty-aware event prediction. *IEEE transactions on pattern analysis and machine intelligence*, 2017a.
- Hossein Soleimani, Adarsh Subbaswamy, and Suchi Saria. Treatment-response models for counterfactual reasoning with continuous-time, continuous-valued interventions. *arXiv preprint arXiv:1704.02038*, 2017b.
- Jos Stam. Stable fluids. In *Proceedings of the 26th annual conference on Computer graphics and interactive techniques*, pages 121–128. ACM Press/Addison-Wesley Publishing Co., 1999.
- Paul Stapor, Fabian Froehlich, and Jan Hasenauer. Optimization and uncertainty analysis of ODE models using second order adjoint sensitivity analysis. *bioRxiv*, page 272005, 2018.
- Jakub M Tomczak and Max Welling. Improving variational auto-encoders using Householder flow. *arXiv preprint arXiv:1611.09630*, 2016.
- Steffen Wiewel, Moritz Becher, and Nils Thuerey. Latent-space physics: Towards learning the temporal evolution of fluid flow. *arXiv preprint arXiv:1802.10123*, 2018.
- Hong Zhang and Adrian Sandu. Fatode: a library for forward, adjoint, and tangent linear integration of ODEs. *SIAM Journal on Scientific Computing*, 36(5):C504–C523, 2014.

Appendix A Proof of the Instantaneous Change of Variables Theorem

Theorem (Instantaneous Change of Variables). *Let $\mathbf{z}(t)$ be a finite continuous random variable with probability $p(\mathbf{z}(t))$ dependent on time. Let $\frac{d\mathbf{z}}{dt} = f(\mathbf{z}(t), t)$ be a differential equation describing a continuous-in-time transformation of $\mathbf{z}(t)$. Assuming that f is uniformly Lipschitz continuous in \mathbf{z} and continuous in t , then the change in log probability also follows a differential equation:*

$$\frac{\partial \log p(\mathbf{z}(t))}{\partial t} = -\text{tr} \left(\frac{df}{d\mathbf{z}}(t) \right)$$

Proof. To prove this theorem, we take the infinitesimal limit of finite changes of $\log p(\mathbf{z}(t))$ through time. First we denote the transformation of \mathbf{z} over an ε change in time as

$$\mathbf{z}(t + \varepsilon) = T_\varepsilon(\mathbf{z}(t)) \quad (14)$$

We assume that f is Lipschitz continuous in $\mathbf{z}(t)$ and continuous in t , so every initial value problem has a unique solution by Picard's existence theorem. We also assume $\mathbf{z}(t)$ is bounded. These conditions imply that f , T_ε , and $\frac{\partial}{\partial \mathbf{z}} T_\varepsilon$ are all bounded. In the following, we use these conditions to exchange limits and products.

We can write the differential equation $\frac{\partial \log p(\mathbf{z}(t))}{\partial t}$ using the discrete change of variables formula, and the definition of the derivative:

$$\frac{\partial \log p(\mathbf{z}(t))}{\partial t} = \lim_{\varepsilon \rightarrow 0^+} \frac{\log p(\mathbf{z}(t)) - \log |\det \frac{\partial}{\partial \mathbf{z}} T_\varepsilon(\mathbf{z}(t))| - \log p(\mathbf{z}(t))}{\varepsilon} \quad (15)$$

$$= - \lim_{\varepsilon \rightarrow 0^+} \frac{\log |\det \frac{\partial}{\partial \mathbf{z}} T_\varepsilon(\mathbf{z}(t))|}{\varepsilon} \quad (16)$$

$$= - \lim_{\varepsilon \rightarrow 0^+} \frac{\frac{\partial}{\partial \varepsilon} \log |\det \frac{\partial}{\partial \mathbf{z}} T_\varepsilon(\mathbf{z}(t))|}{\frac{\partial}{\partial \varepsilon} \varepsilon} \quad (\text{by L'Hôpital's rule}) \quad (17)$$

$$= - \lim_{\varepsilon \rightarrow 0^+} \frac{\frac{\partial}{\partial \varepsilon} |\det \frac{\partial}{\partial \mathbf{z}} T_\varepsilon(\mathbf{z}(t))|}{|\det \frac{\partial}{\partial \mathbf{z}} T_\varepsilon(\mathbf{z}(t))|} \quad \left(\left. \frac{\partial \log(\mathbf{z})}{\partial \mathbf{z}} \right|_{\mathbf{z}=1} = 1 \right) \quad (18)$$

$$= - \underbrace{\left(\lim_{\varepsilon \rightarrow 0^+} \frac{\partial}{\partial \varepsilon} \left| \det \frac{\partial}{\partial \mathbf{z}} T_\varepsilon(\mathbf{z}(t)) \right| \right)}_{\text{bounded}} \underbrace{\left(\lim_{\varepsilon \rightarrow 0^+} \frac{1}{|\det \frac{\partial}{\partial \mathbf{z}} T_\varepsilon(\mathbf{z}(t))|} \right)}_{=1} \quad (19)$$

$$= - \lim_{\varepsilon \rightarrow 0^+} \frac{\partial}{\partial \varepsilon} \left| \det \frac{\partial}{\partial \mathbf{z}} T_\varepsilon(\mathbf{z}(t)) \right| \quad (20)$$

The derivative of the determinant can be expressed using Jacobi's formula, which gives

$$\frac{\partial \log p(\mathbf{z}(t))}{\partial t} = - \lim_{\varepsilon \rightarrow 0^+} \text{tr} \left(\text{adj} \left(\frac{\partial}{\partial \mathbf{z}} T_\varepsilon(\mathbf{z}(t)) \right) \frac{\partial}{\partial \varepsilon} \frac{\partial}{\partial \mathbf{z}} T_\varepsilon(\mathbf{z}(t)) \right) \quad (21)$$

$$= - \text{tr} \left(\underbrace{\left(\lim_{\varepsilon \rightarrow 0^+} \text{adj} \left(\frac{\partial}{\partial \mathbf{z}} T_\varepsilon(\mathbf{z}(t)) \right) \right)}_{=I} \left(\lim_{\varepsilon \rightarrow 0^+} \frac{\partial}{\partial \varepsilon} \frac{\partial}{\partial \mathbf{z}} T_\varepsilon(\mathbf{z}(t)) \right) \right) \quad (22)$$

$$= - \text{tr} \left(\lim_{\varepsilon \rightarrow 0^+} \frac{\partial}{\partial \varepsilon} \frac{\partial}{\partial \mathbf{z}} T_\varepsilon(\mathbf{z}(t)) \right) \quad (23)$$

Substituting T_ε with its Taylor series expansion and taking the limit, we complete the proof.

$$\frac{\partial \log p(\mathbf{z}(t))}{\partial t} = - \text{tr} \left(\lim_{\varepsilon \rightarrow 0^+} \frac{\partial}{\partial \varepsilon} \frac{\partial}{\partial \mathbf{z}} (\mathbf{z} + \varepsilon f(\mathbf{z}(t), t) + \mathcal{O}(\varepsilon^2) + \mathcal{O}(\varepsilon^3) + \dots) \right) \quad (24)$$

$$= - \text{tr} \left(\lim_{\varepsilon \rightarrow 0^+} \frac{\partial}{\partial \varepsilon} \left(I + \frac{\partial}{\partial \mathbf{z}} \varepsilon f(\mathbf{z}(t), t) + \mathcal{O}(\varepsilon^2) + \mathcal{O}(\varepsilon^3) + \dots \right) \right) \quad (25)$$

$$= - \text{tr} \left(\lim_{\varepsilon \rightarrow 0^+} \left(\frac{\partial}{\partial \mathbf{z}} f(\mathbf{z}(t), t) + \mathcal{O}(\varepsilon) + \mathcal{O}(\varepsilon^2) + \dots \right) \right) \quad (26)$$

$$= - \text{tr} \left(\frac{\partial}{\partial \mathbf{z}} f(\mathbf{z}(t), t) \right) \quad (27)$$

□

A.1 Special Cases

Planar CNF. Let $f(\mathbf{z}) = uh(w^T \mathbf{z} + b)$, then $\frac{\partial f}{\partial \mathbf{z}} = u \frac{\partial h^T}{\partial \mathbf{z}}$. Since the trace of an outer product is the inner product, we have

$$\frac{\partial \log p(\mathbf{z})}{\partial t} = -\text{tr} \left(u \frac{\partial h^T}{\partial \mathbf{z}} \right) = -u^T \frac{\partial h}{\partial \mathbf{z}} \quad (28)$$

This is the parameterization we use in all of our experiments.

Hamiltonian CNF. The continuous analog of NICE (Dinh et al., 2014) is a Hamiltonian flow, which splits the data into two equal partitions and is a volume-preserving transformation, implying that $\frac{\partial \log p(\mathbf{z})}{\partial t} = 0$. We can verify this. Let

$$\begin{bmatrix} \frac{d\mathbf{z}_{1:D}}{dt} \\ \frac{d\mathbf{z}_{d+1:D}}{dt} \end{bmatrix} = \begin{bmatrix} f(\mathbf{z}_{d+1:D}) \\ g(\mathbf{z}_{1:D}) \end{bmatrix} \quad (29)$$

Then because the Jacobian is all zeros on its diagonal, the trace is zero. This is a volume-preserving flow.

A.2 Connection to Fokker-Planck and Liouville PDEs

The Fokker-Planck equation is a well-known partial differential equation (PDE) that describes the probability density function of a stochastic differential equation as it changes with time. We relate the instantaneous change of variables to the special case of Fokker-Planck with zero diffusion, the Liouville equation.

As with the instantaneous change of variables, let $\mathbf{z}(t) \in \mathbb{R}^D$ evolve through time following $\frac{d\mathbf{z}(t)}{dt} = f(\mathbf{z}(t), t)$. Then Liouville equation describes the change in density of \mathbf{z} —*a fixed point in space*—as a PDE,

$$\frac{\partial p(\mathbf{z}, t)}{\partial t} = - \sum_{i=1}^D \frac{\partial}{\partial \mathbf{z}_i} [f_i(\mathbf{z}, t)p(\mathbf{z}, t)] \quad (30)$$

However, (30) cannot be easily used as it requires the partial derivatives of $\frac{\partial p(\mathbf{z}, t)}{\partial \mathbf{z}}$, which is typically approximated using finite difference. This type of PDE has its own literature on efficient and accurate simulation (Stam, 1999).

Instead of evaluating $p(\cdot, t)$ at a fixed point, if we follow the trajectory of a particle $\mathbf{z}(t)$, we obtain

$$\begin{aligned} \frac{\partial p(\mathbf{z}(t), t)}{\partial t} &= \underbrace{\frac{\partial p(\mathbf{z}(t), t)}{\partial \mathbf{z}(t)} \frac{\partial \mathbf{z}(t)}{\partial t}}_{\text{partial derivative from first argument, } \mathbf{z}(t)} + \underbrace{\frac{\partial p(\mathbf{z}(t), t)}{\partial t}}_{\text{partial derivative from second argument, } t} \\ &= \sum_{i=1}^D \frac{\partial p(\mathbf{z}(t), t)}{\partial \mathbf{z}_i(t)} \frac{\partial \mathbf{z}_i(t)}{\partial t} - \sum_{i=1}^D \frac{\partial f_i(\mathbf{z}(t), t)}{\partial \mathbf{z}_i} p(\mathbf{z}(t), t) - \sum_{i=1}^D f_i(\mathbf{z}(t), t) \frac{\partial p(\mathbf{z}(t), t)}{\partial \mathbf{z}_i(t)} \\ &= - \sum_{i=1}^D \frac{\partial f_i(\mathbf{z}(t), t)}{\partial \mathbf{z}_i} p(\mathbf{z}(t), t) \end{aligned} \quad (31)$$

We arrive at the instantaneous change of variables by taking the log,

$$\frac{\partial \log p(\mathbf{z}(t), t)}{\partial t} = \frac{1}{p(\mathbf{z}(t), t)} \frac{\partial p(\mathbf{z}(t), t)}{\partial t} = - \sum_{i=1}^D \frac{\partial f_i(\mathbf{z}(t), t)}{\partial \mathbf{z}_i} \quad (32)$$

While still a PDE, (32) can be combined with $\mathbf{z}(t)$ to form an ODE of size $D + 1$,

$$\frac{d}{dt} \begin{bmatrix} \mathbf{z}(t) \\ \log p(\mathbf{z}(t), t) \end{bmatrix} = \begin{bmatrix} f(\mathbf{z}(t), t) \\ - \sum_{i=1}^D \frac{\partial f_i(\mathbf{z}(t), t)}{\partial t} \end{bmatrix} \quad (33)$$

Compared to the Fokker-Planck and Liouville equations, the instantaneous change of variables is of more practical impact as it can be numerically solved much more easily, requiring an extra state of D for following the trajectory of $\mathbf{z}(t)$. Whereas an approach based on finite difference approximation of the Liouville equation would require a grid size that is exponential in D .

Appendix B A Modern Proof of the Adjoint Method

We present an alternative proof to the adjoint method (Pontryagin et al., 1962) that is short and easy to follow.

B.1 Continuous Backpropagation

Let $\mathbf{z}(t)$ follow the differential equation $\frac{d\mathbf{z}(t)}{dt} = f(\mathbf{z}(t), t, \theta)$, where θ are the parameters. We will prove that if we define an adjoint state

$$\mathbf{a}(t) = \frac{dL}{d\mathbf{z}(t)} \quad (34)$$

then it follows the differential equation

$$\frac{d\mathbf{a}(t)}{dt} = -\mathbf{a}(t) \frac{\partial f(\mathbf{z}(t), t, \theta)}{\partial \mathbf{z}(t)} \quad (35)$$

For ease of notation, we denote vectors as row vectors, whereas the main text uses column vectors.

The adjoint state is the gradient with respect to the hidden state at a specified time t . In standard neural networks, the gradient of a hidden layer \mathbf{h}_t depends on the gradient from the next layer \mathbf{h}_{t+1} by chain rule

$$\frac{dL}{d\mathbf{h}_t} = \frac{dL}{d\mathbf{h}_{t+1}} \frac{d\mathbf{h}_{t+1}}{d\mathbf{h}_t}. \quad (36)$$

With a continuous hidden state, we can write the transformation after an ε change in time as

$$\mathbf{z}(t + \varepsilon) = \int_t^{t+\varepsilon} f(\mathbf{z}(t), t, \theta) dt + \mathbf{z}(t) = T_\varepsilon(\mathbf{z}(t), t) \quad (37)$$

and chain rule can also be applied

$$\frac{dL}{d\mathbf{z}(t)} = \frac{dL}{d\mathbf{z}(t + \varepsilon)} \frac{d\mathbf{z}(t + \varepsilon)}{d\mathbf{z}(t)} \quad \text{or} \quad \mathbf{a}(t) = \mathbf{a}(t + \varepsilon) \frac{\partial T_\varepsilon(\mathbf{z}(t), t)}{\partial \mathbf{z}(t)} \quad (38)$$

The proof of (35) follows from the definition of derivative:

$$\frac{d\mathbf{a}(t)}{dt} = \lim_{\varepsilon \rightarrow 0^+} \frac{\mathbf{a}(t + \varepsilon) - \mathbf{a}(t)}{\varepsilon} \quad (39)$$

$$= \lim_{\varepsilon \rightarrow 0^+} \frac{\mathbf{a}(t + \varepsilon) - \mathbf{a}(t + \varepsilon) \frac{\partial}{\partial \mathbf{z}(t)} T_\varepsilon(\mathbf{z}(t))}{\varepsilon} \quad (\text{by Eq 38}) \quad (40)$$

$$= \lim_{\varepsilon \rightarrow 0^+} \frac{\mathbf{a}(t + \varepsilon) - \mathbf{a}(t + \varepsilon) \frac{\partial}{\partial \mathbf{z}(t)} (\mathbf{z}(t) + \varepsilon f(\mathbf{z}(t), t, \theta) + \mathcal{O}(\varepsilon^2))}{\varepsilon} \quad (\text{Taylor series around } \mathbf{z}(t)) \quad (41)$$

$$= \lim_{\varepsilon \rightarrow 0^+} \frac{\mathbf{a}(t + \varepsilon) - \mathbf{a}(t + \varepsilon) \left(I + \varepsilon \frac{\partial f(\mathbf{z}(t), t, \theta)}{\partial \mathbf{z}(t)} + \mathcal{O}(\varepsilon^2) \right)}{\varepsilon} \quad (42)$$

$$= \lim_{\varepsilon \rightarrow 0^+} \frac{-\varepsilon \mathbf{a}(t + \varepsilon) \frac{\partial f(\mathbf{z}(t), t, \theta)}{\partial \mathbf{z}(t)} + \mathcal{O}(\varepsilon^2)}{\varepsilon} \quad (43)$$

$$= \lim_{\varepsilon \rightarrow 0^+} -\mathbf{a}(t + \varepsilon) \frac{\partial f(\mathbf{z}(t), t, \theta)}{\partial \mathbf{z}(t)} + \mathcal{O}(\varepsilon) \quad (44)$$

$$= -\mathbf{a}(t) \frac{\partial f(\mathbf{z}(t), t, \theta)}{\partial \mathbf{z}(t)} \quad (45)$$

We pointed out the similarity between adjoint method and backpropagation (eq. 38). Similarly to backpropagation, ODE for the adjoint state needs to be solved *backwards* in time. We specify the constraint on the last time point, which is simply the gradient of the loss wrt the last time point, and can obtain the gradients with respect to the hidden state at any time, including the initial value.

$$\underbrace{\mathbf{a}(t_N) = \frac{dL}{d\mathbf{z}(t_N)}}_{\text{initial condition of adjoint diffeq.}} \quad \underbrace{\mathbf{a}(t_0) = \int_{t_N}^{t_0} \mathbf{a}(t) \frac{\partial f(\mathbf{z}(t), t, \theta)}{\partial \mathbf{z}(t)} dt}_{\text{gradient wrt. initial value}} \quad (46)$$

Here we assumed that loss function L depends only on the last time point t_N . If function L depends also on intermediate time points t_1, t_2, \dots, t_{N-1} , etc., we can repeat the adjoint step for each of the intervals $[t_{N-1}, t_N]$, $[t_{N-2}, t_{N-1}]$ in the backward order and sum up the obtained gradients.

B.2 Gradients wrt. θ and t

We can generalize (35) to obtain gradients with respect to θ —a constant wrt. t —and the initial and end times, t_0 and t_N . We view θ and t as states with constant differential equations and write

$$\frac{\partial \theta(t)}{\partial t} = \mathbf{0} \quad \frac{dt(t)}{dt} = 1 \quad (47)$$

We can then combine these with z to form an augmented state with corresponding differential equation and adjoint state,

$$\frac{d}{dt} \begin{bmatrix} z \\ \theta \\ t \end{bmatrix} (t) = f_{aug}([z, \theta, t]) := \begin{bmatrix} f([z, \theta, t]) \\ \mathbf{0} \\ 1 \end{bmatrix}, \quad \mathbf{a}_{aug} := \begin{bmatrix} \mathbf{a} \\ \mathbf{a}_\theta \\ \mathbf{a}_t \end{bmatrix}, \quad \mathbf{a}_\theta(t) := \frac{dL}{d\theta(t)}, \quad \mathbf{a}_t(t) := \frac{dL}{dt(t)} \quad (48)$$

Note this formulates the augmented ODE as an autonomous (time-invariant) ODE, but the derivations in the previous section still hold as this is a special case of a time-variant ODE. The Jacobian of f has the form

$$\frac{\partial f_{aug}}{\partial [z, \theta, t]} = \begin{bmatrix} \frac{\partial f}{\partial z} & \frac{\partial f}{\partial \theta} & \frac{\partial f}{\partial t} \\ \mathbf{0} & \mathbf{0} & \mathbf{0} \\ \mathbf{0} & \mathbf{0} & \mathbf{0} \end{bmatrix} (t) \quad (49)$$

where each $\mathbf{0}$ is a matrix of zeros with the appropriate dimensions. We plug this into (35) to obtain

$$\frac{d\mathbf{a}_{aug}(t)}{dt} = -[\mathbf{a}(t) \quad \mathbf{a}_\theta(t) \quad \mathbf{a}_t(t)] \frac{\partial f_{aug}}{\partial [z, \theta, t]}(t) = -[\mathbf{a} \frac{\partial f}{\partial z} \quad \mathbf{a} \frac{\partial f}{\partial \theta} \quad \mathbf{a} \frac{\partial f}{\partial t}](t) \quad (50)$$

The first element is the adjoint differential equation (35), as expected. The second element can be used to obtain the total gradient with respect to the parameters, by integrating over the full interval.

$$\frac{dL}{d\theta} = \int_{t_N}^{t_0} \mathbf{a}(t) \frac{\partial f(\mathbf{z}(t), t, \theta)}{\partial \theta} dt \quad (51)$$

Note the negative sign cancels out since we integrate backwards from t_N to t_0 . Finally, we also get gradients with respect to t_0 and t_N , the start and end of the integration interval.

$$\frac{dL}{dt_N} = -\mathbf{a}(t_N) \frac{\partial f(\mathbf{z}(t_N), t_N, \theta)}{\partial t_N} \quad \frac{dL}{dt_0} = \int_{t_N}^{t_0} \mathbf{a}(t) \frac{\partial f(\mathbf{z}(t), t, \theta)}{\partial t} dt \quad (52)$$

Between (35), (46), (51), and (52) we have gradients for all possible inputs to an initial value problem solver.

Appendix C Autograd Implementation

```
import scipy.integrate

import autograd.numpy as np
from autograd.extend import primitive, defvjp_argnums
from autograd import make_vjp
from autograd.misc import flatten
from autograd.builtins import tuple

odeint = primitive(scipy.integrate.odeint)

def grad_odeint_all(yt, func, y0, t, func_args, **kwargs):
    # Extended from "Scalable Inference of Ordinary Differential
    # Equation Models of Biochemical Processes", Sec. 2.4.2
    # Fabian Froehlich, Carolin Loos, Jan Hasenauer, 2017
    # https://arxiv.org/pdf/1711.08079.pdf

    T, D = np.shape(yt)
    flat_args, unflatten = flatten(func_args)

    def flat_func(y, t, flat_args):
        return func(y, t, *unflatten(flat_args))

    def unpack(x):
        # y, vjp_y, vjp_t, vjp_args
        return x[0:D], x[D:2 * D], x[2 * D], x[2 * D + 1:]

    def augmented_dynamics(augmented_state, t, flat_args):
        ...

Note that we've overloaded  $t$  to be both a part of the state and the (dummy) independent variable. The distinction is clear given context, so we keep  $t$  as the independent variable for consistency with the rest of the text.
```

```

# Orginal system augmented with vjp_y , vjp_t and vjp_args .
y, vjp_y, _, _ = unpack(augmented_state)
vjp_all, dy_dt = make_vjp(flat_func, argnum=(0, 1, 2))(y, t, flat_args)
vjp_y, vjp_t, vjp_args = vjp_all(-vjp_y)
return np.hstack((dy_dt, vjp_y, vjp_t, vjp_args))

def vjp_all(g,**kwargs):
    vjp_y = g[-1, :]
    vjp_t0 = 0
    time_vjp_list = []
    vjp_args = np.zeros(np.size(flat_args))

    for i in range(T - 1, 0, -1):
        # Compute effect of moving current time.
        vjp_cur_t = np.dot(func(yt[i, :], t[i], *func_args), g[i, :])
        time_vjp_list.append(vjp_cur_t)
        vjp_t0 = vjp_t0 - vjp_cur_t

        # Run augmented system backwards to the previous observation.
        aug_y0 = np.hstack((yt[i, :], vjp_y, vjp_t0, vjp_args))
        aug_ans = odeint(augmented_dynamics, aug_y0,
                          np.array([t[i], t[i - 1]]), tuple((flat_args,)), **kwargs)
        _, vjp_y, vjp_t0, vjp_args = unpack(aug_ans[1])

        # Add gradient from current output.
        vjp_y = vjp_y + g[i - 1, :]

    time_vjp_list.append(vjp_t0)
    vjp_times = np.hstack(time_vjp_list)[::-1]

    return None, vjp_y, vjp_times, unflatten(vjp_args)
return vjp_all

def grad_argnums_wrapper(all_vjp_builder):
    # A generic autograd helper function. Takes a function that
    # builds vjps for all arguments, and wraps it to return only required vjps.
    def build_selected_vjps(argnums, ans, combined_args, kwargs):
        vjp_func = all_vjp_builder(ans, *combined_args, **kwargs)
        def chosen_vjps(g):
            # Return whichever vjps were asked for.
            all_vjps = vjp_func(g)
            return [all_vjps[argnum] for argnum in argnums]
        return chosen_vjps
    return build_selected_vjps

def vjp_argnums(odeint, grad_argnums_wrapper(grad_odeint_all))
```

Appendix D Algorithm for training the latent ODE model

To obtain the latent representation \mathbf{z}_{t_0} , we traverse the sequence using RNN and obtain parameters of distribution $q(\mathbf{z}_{t_0} | \{\mathbf{x}_{t_i}, t_i\}_i, \theta_{enc})$. The algorithm follows a standard VAE algorithm with an RNN variational posterior and an ODESolve model:

1. Run an RNN encoder through the time series and infer the parameters for a posterior over \mathbf{z}_{t_0} :

$$q(\mathbf{z}_{t_0} | \{\mathbf{x}_{t_i}, t_i\}_i, \phi) = \mathcal{N}(\mathbf{z}_{t_0} | \mu_{\mathbf{z}_{t_0}}, \sigma_{\mathbf{z}_{t_0}}), \quad (53)$$

where $\mu_{\mathbf{z}_{t_0}}, \sigma_{\mathbf{z}_{t_0}}$ comes from hidden state of $RNN(\{\mathbf{x}_{t_i}, t_i\}_i, \phi)$

2. Sample $\mathbf{z}_{t_0} \sim q(\mathbf{z}_{t_0} | \{\mathbf{x}_{t_i}, t_i\}_i)$
3. Obtain $\mathbf{z}_{t_1}, \mathbf{z}_{t_2}, \dots, \mathbf{z}_{t_M}$ by solving ODE ODESolve($\mathbf{z}_{t_0}, f, \theta_f, t_0, \dots, t_M$), where f is the function defining the gradient $d\mathbf{z}/dt$ as a function of \mathbf{z}

4. Maximize ELBO = $\sum_{i=1}^M \log p(\mathbf{x}_{t_i} | \mathbf{z}_{t_i}, \theta_x) + \log p(\mathbf{z}_{t_0}) - \log q(\mathbf{z}_{t_0} | \{\mathbf{x}_{t_i}, t_i\}_i, \phi)$,
 where $p(\mathbf{z}_{t_0}) = \mathcal{N}(0, 1)$

Appendix E Extra Figures

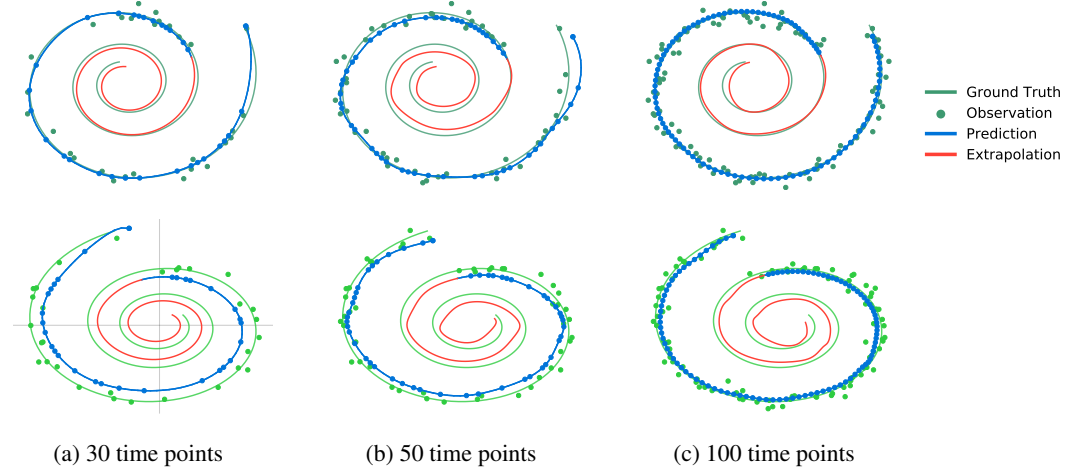


Figure 10: Spiral reconstructions using a latent ODE with a variable number of noisy observations.